Atom lithography with metastable helium

Claire S. Allred, Jason Reeves, Christopher Corder, and Harold Metcalf[a)]
Physics and Astronomy, Stony Brook University, Stony Brook. New York 11794-3800, USA

(Received 14 July 2009; accepted 23 December 2009; published online 12 February 2010)

A bright metastable helium (He^*) beam is collimated sequentially with the bichromatic force and three optical molasses velocity compression stages. Each He^* atom in the beam has 20 eV of internal energy that can destroy a molecular resist assembled on a gold coated silicon wafer. Patterns in the resist are imprinted onto the gold layer with a standard selective etch. Patterning of the wafer with the He^* was demonstrated with two methods. First, a mesh was used to protect parts of the wafer making an array of grid lines. Second, a standing wave of $\lambda = 1083$ nm light was used to channel and focus the He^* atoms into lines separated by $\lambda/2$. The patterns were measured with an atomic force microscope establishing an edge resolution of 80 nm. Our results are reliable and repeatable.
 [doi:10.1063/1.3295903]

I. INTRODUCTION

The ability to record and preserve the positions of atoms in a permanent structure on a submicron scale has myriad of possible applications. To begin, the structure itself may be of value. Such nanoscale patterns, whose spacing is known to spectroscopic precision, can be made with precise long-range regularity. Examples include gratings for short wavelength radiation, standards for microscope calibration, photonic crystals, metamaterial samples, and many others. Second, the distribution of atoms is determined by light fields so that the pattern produced can be used as a measure of the light intensity distribution. For example, very small deviations caused by wave front imperfections could be detected. Finally, the process by which the light fields influence the atomic motion in forming such patterns is an interesting topic of study by itself.

We report here nanolithography using neutral atoms in a previous unreported range of parameters. In particular, the two domains of laser intensity used for steering the atoms into the desired patterns are called the focusing and channeling regimes, and our experiments include the low intensity focusing regime. Although our numerical simulations of such focusing by a standing wave suggest that we cannot produce patterns when the atomic beam has a relatively large angular divergence, we have collimated our beam sufficiently to accomplish such patterning in this regime. Smaller features can be obtained in the focusing regime than in the channeling regime.[1]

The first demonstration of atomic nanofabrication using light fields to steer the atoms was described by Timp *et al.*[2] with a beam of sodium atoms deposited on a glass substrate. Because of the chemical instability of sodium in air, their fabricated structure could not survive removal from the vacuum chamber. Later the direct deposition of more stable atoms was explored, with extensive demonstrations in chromium.[3–5] The structures fabricated with such direct deposition techniques are limited to atoms with readily accessible optical transitions for interaction with laser fields.

By contrast, lithographic techniques can be used to make nanoscale patterns with a greater diversity of materials. This is because the patterning is done by optically controlling atoms that are different from the eventual fabricated material. The only requirement on these materials is their vulnerability or resistance to an appropriate chemical etch. Thus very many materials can be patterned for fabrication. A review of both direct deposit and lithographic techniques appeared in 2003.[6]

Our atom lithography (positive resist) is achieved by destroying the chemical bonds in a layer of polymeric molecules of self-assembled monolayers (SAMs), dissolving the damaged molecules, and finally etching the exposed area. The metastable $2\,^3S$ state of helium (He^*) is ideal for this because its internal energy of 20 eV is higher than any other metastable atom. Thus it is most effective for exposing a resist with minimum dosage and results in the shortest exposure time, requiring minimum restrictions on the atomic beams and laser control.[6]

The use of He^* to make such chemical modification to a surface resist for later etching was reported in 1995 in Refs. 7–9, but these authors used the shadow of a mechanical mask to make their patterns. Soon afterward, metastable Ar was also used.[10] The first use of optical fields to steer and channel He^* atoms was reported in 2004.[11] The resulting fabricated arrays have intrinsic nanometer dimensions since the typical scale of optical interferences is of the order of half a wavelength, i.e., in the sub-μm domain.

II. NUMERICAL CALCULATIONS

In preparation for our experiments, we did several numerical calculations to determine the neighborhood of our operating parameters. The first of these were simple trajectories of atoms incident perpendicular to a standing wave with transverse Gaussian intensity distribution. We found trajectories corresponding to both the focusing and channeling regimes, and especially had a close look at the region between them. All these trajectories looked very similar to those published elsewhere.[3,4]

[a)]Electronic mail: hmetcalf@notes.cc.sunysb.edu.

Since our initial choice for trajectory calculations of a perfectly collimated, monovelocity beam incident exactly perpendicular to the patterning beam axis is unrealistic, we also performed a Monte Carlo simulation of the paths and landing points of the atoms. The single longitudinal and transverse atomic beam velocities were replaced by distributions. The longitudinal velocity distribution was based on time-of-flight measurements of the atomic beam. The transverse velocity distribution was estimated using the change in atomic beam spot size correlated with the longitudinal velocity.

The simulation results in the channeling regime showed the formation of half-wavelength spaced structures over a wide range of parameters. However, we found that in the focusing regime, for the parameters estimated from our experimental setup, there was no patterning. The simulations indicated that pattern formation was more sensitive to atomic beam transverse velocity than to the longitudinal velocity distribution,[6] and reducing the transverse velocity indeed resulted in patterning even in the focusing regime. Like the trajectory calculations, the results of these Monte Carlo simulations differed very little from those previously published.[3,4]

III. EXPERIMENT

Our neutral atom lithography experiments use a bright beam of He^* that originates from a reverse flow dc discharge source.[12,13] It has a slightly supersonic longitudinal velocity distribution centered near $v_\ell = 1125$ m/s and is about ± 200 m/s wide. This atomic beam is collimated with the bichromatic force,[14,15] followed by three optical molasses velocity compression stages.[16] Because bichromatic collimation makes such an intense He^* beam, our exposure time is measured in minutes instead of hours. We have observed the focusing and channeling of the He^* beam by the dipole force the atoms experience while traversing a standing wave of light.

In our experiment the bichromatic force is implemented with counterpropagating light beams, each containing two frequencies that are detuned from atomic resonance by $\pm\delta = 2\pi \times 60$ MHz. All the light originates from diode lasers stabilized by saturated absorption spectroscopy, frequency shifted by various acousto-optic modulators, and amplified by Yb-doped fiber amplifiers. The laser linewidths, both before and after the fiber amplifiers, are measured by heterodyne spectroscopy to be less than 0.25 MHz, about 1/6 of the natural width $\gamma \equiv 1/\tau = 2\pi \times 1.6$ MHz.

With the frequencies of these beams centered about the atomic resonance, the dependence of the force on atomic velocity v is symmetric about $v=0$ over the velocity range $\pm\delta/2k$, and nearly vanishes elsewhere.[14] Since collimation requires a force that is antisymmetric about $v=0$, we shift the velocity dependence by $\delta/2k$ without changing its shape by shifting the laser frequencies appropriately.[15] The resulting force is unidirectional so that collimation requires two regions for each of two dimensions, making four bichromatic force regions.

The four sequential bichromatic force regions are placed as close as possible to the point where the cone of He^* atoms emerges from the source so that the collimated beam has a minimum diameter.[16] The apodized Gaussian beam profiles in each 10 mm long region carry an average intensity of $\sim 4000\ I_s$, where the saturation intensity $I_s \equiv \pi hc/3\lambda^3\tau \approx 0.17$ mW/cm^2.

The transverse velocity spread after the bichromatic force regions is well above ± 10 m/s corresponding to $\sim \pm 9$ mrad, and is not suitable for our purposes. Therefore we have a "booster" molasses stage with detuning many times larger than γ to capture atoms in this large angular spread, followed by an ordinary Doppler molasses to reduce the atomic beam divergence to nearly 3 mrad with very little loss of atoms. These molasses regions have a length along the beam line of ≈ 19 and ≈ 9 mm, respectively. A bit further down the line is one-dimensional Doppler molasses used to steer the atoms and determine their angle of incidence at the target. This reduces the divergence of the atomic beam in the patterning dimension to ~ 1 mrad. The Doppler limit corresponds to ~ 0.25 mrad, but is not achieved here because the interaction time is somewhat less than only a single molasses damping time, and there are many atoms outside the velocity capture range of the Doppler molasses whose transverse velocity is reduced but they are certainly not truly damped so they contribute to a broader velocity distribution.

This collimation section occupies 8.2 cm of our beamline and delivers $\sim 1.5 \times 10^9$ atoms/s mm^2 at our sample, 68 cm from the He^* source.[16] Thus a 10 min exposure deposits one He^* in each ~ 1 nm^2 area without any focusing, and the focusing could easily increase this dosage to a few He^* per SAM molecule site (estimated area ~ 0.3 nm^2). These dosages are known to $\pm 10\%$, and this limit arises from fluctuations of the laser beams that collimate the atoms. Note that He^* can eject electrons from the stainless steel surface of one of our detectors with a measured 75% efficiency.[17]

Our beam of He^* atoms is focused into lines by a standing wave field of $\lambda = 1083$ nm light tuned ~ 490 MHz above the $2\,^3S_1 \rightarrow 2\,^3P_2$ transition (atoms attracted toward its nodes). It has an elliptical cross section with waist of $w_\parallel \sim 1.5$ mm parallel to the substrate surface and $w_\ell \sim 330\ \mu$m along the atomic beam path.

We describe the incident power of the traveling wave P_{inc} that is retroreflected to form this "optical mask" in terms of the power that focuses the atoms on its resulting standing wave axis: $P_{\text{focus}} = 4.22 I_s \Delta (v_\ell \tau)^2/\omega_r$ taken from Eq. 23 of Ref. 4 for the case of a round Gaussian beam, where Δ is the detuning from the atomic resonance and $\omega_r \equiv \hbar k^2/2M$ is the recoil frequency. It is important to note that P_{focus} for such a beam is independent of its waist size. Our light mask is elliptical so we write $P'_{\text{focus}} = P_{\text{focus}}(w_\parallel/w_\ell) \approx 5.0$ mW.

The patterning force on the atoms derives from the gradient of the standing wave whose peak intensity I_{peak} is given by four times the peak intensity of the incident traveling wave $2P_{\text{inc}}/A$ because the amplitudes add ($A = \pi w_0^2$ for a circular beam). Thus $I_{\text{focus}} = 4 \times [2P'_{\text{focus}}/(\pi w_\ell w_\parallel)] \approx 2.42$ W/cm$^2 \approx 1.4 \times 10^4 I_s$. The excitation rate is $\gamma/50$ corresponding to 16 times the beam traversal time so that spon-

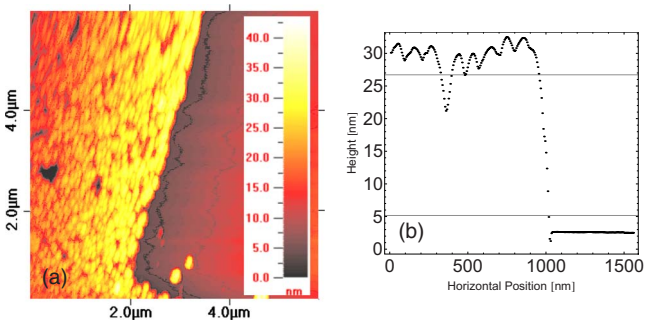

FIG. 1. (Color online) An AFM image near the corner of the shadow of the mesh. Part (a) shows one corner of the mesh image that is located near the bottom center of the picture, and a depth scale. Part (b) shows a 1.5-μm-wide trace across the edge averaged over about 5% of the image height corresponding to 0.3 mm located about 3/4 of the way up from the bottom of the image.

taneous emission is negligible. The peak intensity I_{peak} of our standing wave is varied from I_{focus} to over 15 W/cm^2, slightly into the channeling regime.[4]

Our samples are built on single-crystal silicon wafers that have a 20 nm layer of gold evaporated onto their [100] surface over a 0.5 nm chromium adhesion layer. These wafers are grown and coated commercially. The SAM is deposited onto the gold surface by submersing the wafer in a 1 mM solution of nonanethiol in ethanol for 13–20 h. The long chain molecules orient themselves with their hydrophillic tails bound to the gold substrate and their hydrophobic heads sticking out into the solution. The incident He* attacks the structure of the SAM molecules thereby making them soluble in a wet chemical etch. Then the unprotected gold regions are dissolved in a subsequent etch while the undisturbed SAM protects the remaining pattern in the gold layer.

IV. RESULTS

Our first samples were exposed using a Ni mesh as a physical mask. The left side of Fig. 1 shows an atomic force microscope (AFM) image of one small region near the corner of the shadow of the mesh, and the right side shows a trace over the edge of the structure. From this plot we estimate the edge resolution to be ~80 nm. This resolution seems to be limited by the domain granularity of the gold layer and by the etching process (but not by the etching time). This method of neutral atom lithography is analogous to ordinary resist-based technologies that are used in most conventional lithography processes.

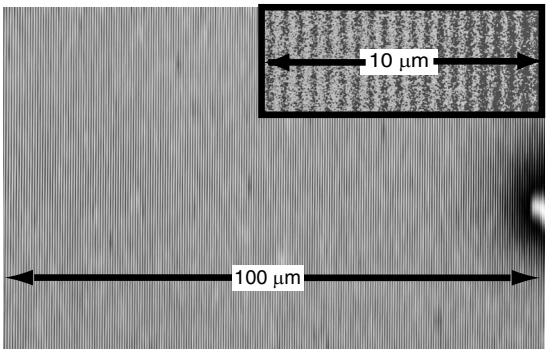

FIG. 2. SEM image of one sample. There are ~200 vertical lines on this figure separated by 541.7 nm=λ/2. The unfocused peak dosage was 3 $\times 10^{12}$ atoms/mm^2 during the 31 min exposure. I_{peak} of the light mask beam used for patterning was nearly 6 W/cm^2. It has been digitally smoothed for reproduction since aliasing of the image in print or on screen may cause deception. The inset shows a small portion magnified by 5 but with no smoothing.

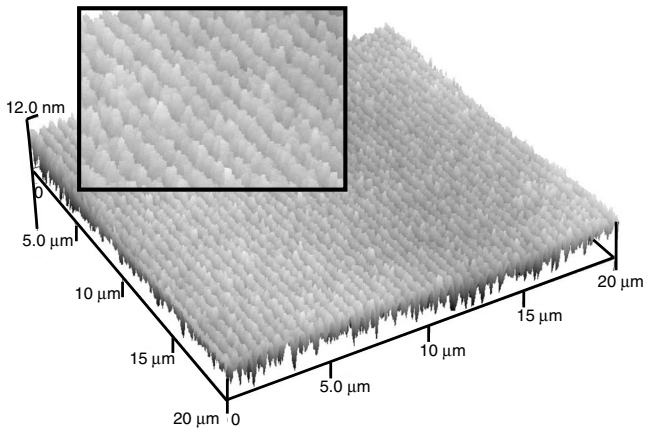

FIG. 3. AFM image of the same wafer as Fig. 2. This image has a 5 point smoothing but still clearly shows both the graininess of the original gold coating and the resolution of the AFM.

A. Low power channeling mask

Samples patterned with an "optical mask" (standing light wave) in the channeling regime produced the expected array of lines covering the full 3×3 mm exposed region of the substrate. The entire area is patterned with uniformly spaced lines in gold. Figure 2 shows ~200 gold lines spanning about 100×65 μm of this region (less than 1/1000 of the total area). The power of the light mask beam used for this sample was ~14 mW$\approx 2.8P'_{\text{focus}}$ or $I_{\text{peak}}\approx 6$ W/cm^2. It was cut in the middle by the substrate, as on the left side of Fig. 3 of Ref. 6. Thus its width is 3 mm along the surface perpendicular to its $\vec{k}$ vectors (twice the waist), and the atoms travel ~330 μm through half of it before hitting the SAM-coated substrate.

Figure 3 shows the AFM image of the same sample. This angular view shows that the depth of the lines is approximately 10 nm and that the spatial resolution is limited by its graininess to about 1/5 of the line separation, 100 nm, consistent with the ~80 nm resolution shown in Fig. 1. Figure 4 shows a plot of a single trace across the AFM image of Fig. 3. It has deep valleys where the He* atoms were concentrated by focusing of the light mask, and large quasiflat areas between the valleys.

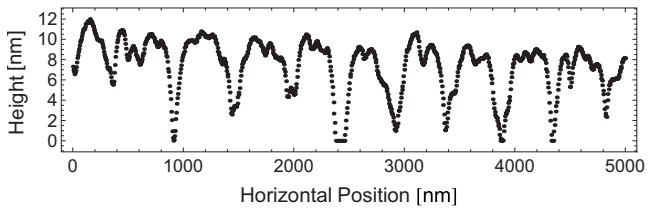

FIG. 4. Plot of a single trace across the AFM image of Fig. 3. This trace is taken of the raw image with no smoothing, only tilt removal from the AFM.

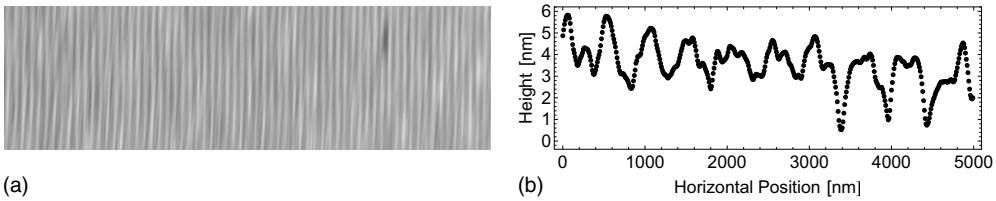

FIG. 5. Part (a) shows a small region of the patterned area produced by a light mask whose intensity was in the focusing regime. The image has been digitally smoothed for clarity in print. Part (b) shows a plot of the AFM image of the raw data averaged over 10% of the image height (1 μm of the 10 μm scan).

The reduction in patterning depth from that of the mesh mask arises from the difference between mechanically blocking and optically steering the atoms. The mesh mask completely blocks atoms from the shadowed regions, while the light mask channels atoms into the pattern efficiently but not completely. Thus there will be atoms that are outside the channeling ability of the light mask that contribute to an exposure outside the feature areas. This will reduce the etching depth of the samples.

The average full width at half depth of the valleys between our lines produced with a light mask is 100 nm as shown in Fig. 4, and is comparable to that previously reported.[11] This, along with the edge width results that are shown for our mesh mask exposures in Fig. 1, suggest that the resolution of our technique is limited by the sample processing methods. The results described up to here are comparable to those achieved by previous workers, but our exposure times are generally shorter because our He^* beam is brighter.

B. Focusing mask

The previously published work on Ne^* in Ref. 10 and He^* in Ref. 11 were done with light mask powers that were 250–350 times P_{focus}. The work described in Ar^* in Ref. 18 was done at a lower power, but the light mask was used to both quench and focus the atoms, and as such allowed for lower intensity. This is because the quenching in a standing wave affects the atoms that focus most poorly because they are most susceptible to spherical aberrations. Of course, this quenching reduced the number of metastable atoms and resulted in much longer exposure time. The $2\,^3S_1$ state of He does not have an available quenching transition, and the use of low intensity masks to pattern He^* has not been demonstrated to our knowledge.

We report here patterning with an optical mask in the focusing regime for the first time. We can do this because our third optical molasses stage provides additional collimation that enables the formation of these nanostructures with much lower light intensity in the optical mask. Ultimately such patterning in the focusing regime would allow for the production of smaller features.

Our measured He^* beam profile after this third stage is elliptical with half-axes 1.3 by 1.2 mm. The third molasses stage collimates only the horizontal spreading of the beam, so at a distance 123 cm from the molasses region it expands to only 2.7 mm while the vertical dimension expands to 5.1 mm. This corresponds to a divergence of 1.1 mrad in the patterning dimension. However, this divergence may not accurately estimate the transverse velocity of the atomic beam since its finite initial size may cause the transverse velocity distribution to be spatially dependent. Contrary to the reports of earlier workers, this transverse velocity distribution is narrow enough to make patterns with much lower intensity in the light mask. Thus we have demonstrated a patterning technique for He^* in a frequency and power regime previously stated to be inaccessible.

The power of the beam used to form the structures shown in Fig. 5 was $\approx P'_{\text{focus}}$ and the exposure time was $\sim$48 min. Our numerical simulations do not give patterning for these beam parameters. We suspect the estimate of the width of the transverse velocity distribution based on the longitudinally correlated, spatial divergence measurements overestimate the actual transverse velocity spread of the atomic beam. By using lower transverse velocity spreads in the numerical simulations there is better agreement between simulation and experimental results.

It is easily noticeable that the depth of the features changes from the channelling regime (shown in Fig. 4) to the focusing regime (shown in Fig. 5). The focusing light intensity requires a narrower transverse velocity distribution for the atoms to land in the desired locations. This restriction means that atoms are less effectively concentrated into lines. The concentration difference between desired area and nondesired area is now smaller, limiting how well the SAM protects the gold and thus affecting the etching procedure.

C. Analysis of results

Analysis of all of our light mask samples begins with spatial fast Fourier transforms (FFT) of the images from both AFM and scanning electron microscope (SEM) scans of our samples. We do FFTs using a standard MATHEMATICA routine. These transforms allow for an accurate measurement of the periodicity and give us an understanding of the shapes of periodic structures. Even in samples where the pattern is difficult to see in the images by eye, the peaks in the FFTs clearly reveal the presence of the nanoscale structures.

The fundamental frequency is always visible in the FFTs of the samples with patterning. The periodicity is determined by measuring the separation between the peaks that appear at positive and negative frequencies. These measurements from the AFM scans have consistently returned a line spacing with a standard deviation of $\pm 1\%$ regardless of light mask power or exposure time. Needless to say, the spectroscopically known accuracy of our line spacing is significantly higher than that of the calibration samples provided by the AFM manufacturer. The precision depends upon substrate stability, thermal properties, etc.

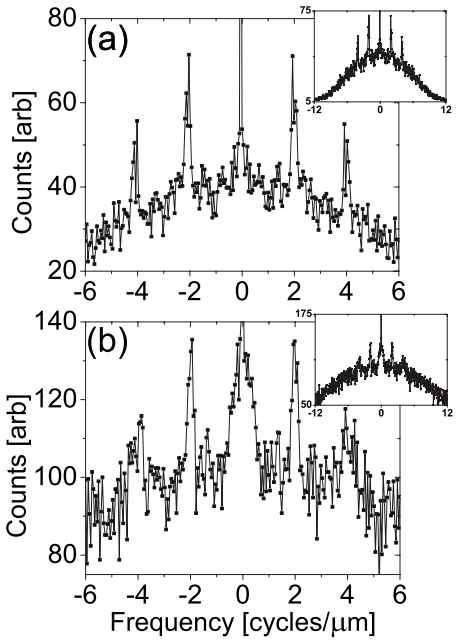

FIG. 6. These plots show traces across a single narrow swath of the 2D FFTs from 20 μm long regions of our samples. They clearly show the fundamental at about 2 cycles/μm and the second harmonics at twice this spacing. The insets comprise a much wider part of the scan to show the absence of higher frequency peaks. The peak widths reflect the presence of only 40 nanolines in the 20 μm scans. The plots were taken from raw data, with no smoothing, filtering, tilt removal, or other processing. Part (a) is from the same channeling regime sample as Figs. 2–4 but could have been from any one of many samples. Part (b) is from the same sample as shown in Fig. 5 and shows somewhat weaker second harmonic peaks, consistent with Fig. 5.

In addition to the fundamental frequency that is always visible in the FFT, we typically also see somewhat weaker second and/or third harmonic peaks. The presence of these higher harmonics, and their relative amplitudes, give information on the exposure and etching parameters. The atomic beam and light mask both have transverse Gaussian cross sections resulting in different atomic dosages and light intensities across the exposed region. The sample is etched in solution until the silicon is visible in the region defined by the peak of the atomic beam. In areas that are etched deeper, the presence of the higher harmonics indicate the structures are scalloped and somewhat square in shape, as shown in Fig. 4. In regions that correspond to less etched areas, as in the case of low atomic dosage and low light intensity, we tend to see the presence of the first harmonic only. Even though the atomic beam dosage, light intensity, and thickness of the gold varies across each sample and slightly from sample to sample, we have reliably seen uniformly spaced lines whose separation is known with spectroscopic precision. The widths of all the peaks are transform limited to the best of our ability to measure.

Figure 6 shows traces across the horizontal axis of the two-dimensional (2D) FFTs. Part (a) is from the same sample as in Figs. 2–4. As we might expect from the flat top and deep valleys shown in Fig. 4, there is a strong fundamental and second harmonic, but higher order harmonics are buried in the noise. Although we have chosen to use this same sample in all four of these figures, it should be pointed out that we could have chosen any one of dozens of samples to present here and found essentially the same results. Part (b) of Fig. 6 is from the same sample as shown in Fig. 5, but is otherwise similar to part (a). Here the second harmonic is smaller relative to the fundamental, consistent with the trace shown in the lower part of Fig. 5. The flat tops and deep valleys are not as well defined there, and so the second harmonic is weaker in the spatial spectrum. The narrow peak at zero frequency and the broad hump underneath the narrow peaks are artifacts from the global tilt of the samples in the AFM stage, the finite size of the images, the gold granularity, the sharp cutoffs at their edges, and unavoidable long-range waviness of the AFM scans.

We have done some filtering and band-pass blocking on a few of the FFT plots and can display clear peaks on a flat baseline, but these are not shown here. The clearly defined structures of Fig. 5 and the strong peaks in part (b) of Fig. 6 demonstrate unequivocally that we have accomplished atomic nanolithography with our He^* beam using an optical mask whose power is in the focusing regime.

V. CONCLUSION

Our fabrications have reliably and repeatably created uniformly spaced lines whose separation is known with spectroscopic precision, sample after sample, over a period of months. Moreover, we have made AFM scans on some of them as late as nine months after they were fabricated, and the patterns do not show any sign of deterioration: they are indistinguishable from the original images.

In a standing wave arranged to channel the He^* into lines separated by $\lambda/2$ on the sample, our lines cover the entire exposed length of the substrate, about 3 mm. They are 3 mm long, corresponding to about twice the beam waist of the laser standing wave. In the focusing regime the pattern also covered the entire exposed area of the sample, and we emphasize that this is an unexplored region of parameters that was previously thought not to work at all. Thus we have reliably produced structures less than 300 nm wide, separated by 541.5 nm, with ~6000 lines of length ~2800λ.[16] The edge resolution of well under 100 nm suggests that we are capable of smaller structures, and He^* lends itself to such fabrication because of the $\lambda = 389$ nm transition to the $3\,^3P$ states.

ACKNOWLEDGMENTS

We acknowledge very helpful discussions with K.A.H. van Leeuwen. This work supported by the O.N.R.

[1] W. R. Anderson, C. C. Bradley, J. J. McClelland, and R. J. Celotta, Phys. Rev. A **59**, 2476 (1999).
[2] G. Timp, R. E. Behringer, D. M. Tennant, J. E. Cunningham, M. Prentiss, and K. K. Berggren, Phys. Rev. Lett. **69**, 1636 (1992).
[3] J. J. McClelland, R. E. Scholten, E. C. Palm, and R. Celotta, Science **262**, 877 (1993).
[4] J. J. McClelland, J. Opt. Soc. Am. B **12**, 1761 (1995).
[5] R. Gupta, J. J. McClelland, Z. J. Jabbour, and R. Celotta, Appl. Phys. Lett. **67**, 1378 (1995).
[6] D. Meschede and H. Metcalf, J. Phys. D: Appl. Phys. **36**, R17 (2003).
[7] K. K. Berggren, A. Bard, J. L. Wilbur, J. D. Gillaspy, A. G. Helg, J. J. McClelland, S. L. Rolston, W. D. Phillips, M. Prentiss, and G. M. Whitesides, Science **269**, 1255 (1995).

[8]S. Nowak, T. Pfau, and J. Mlynek, Appl. Phys. B: Lasers Opt. **63**, 203 (1996).
[9]B. Brezger, T. Schulze, U. Drodofsky, J. Stuhler, S. Nowak, T. Pfau, and J. Mlynek, J. Vac. Sci. Technol. B **15**, 2905 (1997).
[10]K. S. Johnson, J. H. Thywissen, N. H. Dekker, K. K. Berggren, A. P. Chu, R. Younkin, and M. Prentiss, Science **280**, 1583 (1998).
[11]S. Petra, L. Feenstra, W. Hogervorst, and W. Vassen, Appl. Phys. B: Lasers Opt. **78**, 133 (2004).
[12]J. Kawanaka, M. Hagiuda, K. Shimizu, F. Shimizu, and H. Takuma, Appl. Phys. B: Lasers Opt. **56**, 21 (1993).
[13]H. Mastwijk, M. van Rijnbach, J. Thomsen, P. van der Straten, and A. Niehaus, Eur. Phys. J. D **4**, 131 (1998).
[14]J. Söding, R. Grimm, Y. Ovchinnikov, P. Bouyer, and C. Salomon, Phys. Rev. Lett. **78**, 1420 (1997).
[15]M. Partlow, X. Miao, J. Bochmann, M. Cashen, and H. Metcalf, Phys. Rev. Lett. **93**, 213004 (2004).
[16]C. Allred, Ph.D. thesis, Stony Brook University, 2009.
[17]F. B. Dunning, R. D. Rundel, and R. F. Stebbings, Rev. Sci. Instrum. **46**, 697 (1975).
[18]P. Engels, S. Salewski, H. Levsen, K. Sengstock, and W. Ertmer, Appl. Phys. B: Lasers Opt. **69**, 407 (1999).